Materials Horizons

Accepted Manuscript

ROYAL SOCIETY OF CHEMISTRY

rsc.li/materials-horizons

A Graphene-like Metallic Cathode Host For Long-life and High-loading Lithium-Sulfur Batteries

Quan Pang, Dipan Kundu, and Linda F. Nazar*

Department of Chemistry and the Waterloo Institute for Nanotechnology, University of Waterloo, 200 University Ave W, Waterloo, Ontario N2L 3G1, Canada. Email: lfnazar@uwaterloo.ca

ABSTRACT: Development of Li-S batteries with long cycle life and high practical capacity is central to enable low-cost, large-scale energy storage. Sulfiphilic cathode materials with strong affinity for lithium (poly)sulfides are a promising new group of candidates to control dissolution/precipitation reactions in the cell, where the improvement of conductivity and the areal sulfur loading is an important objective. Here we report a metallic Co_9S_8 material with an interconnected graphene-like nano-architecture to realize this aim. First-principles calculations coupled with spectroscopic evidence demonstrate the synergistic strong dual-interactions of polysulfides with the host. The three dimensional interconnected structure with hierarchical porosity not only manifests up to a factor of 10 increase of cycling stability (fade < 0.045% per cycle over 1500 cycles at C/2) compared to standard porous carbons but also, more importantly, enables a high-loading sulfur electrode with up to 75 wt% sulfur, and up to 4.5 mg cm^{-2} areal sulfur loading.

KEYWORDS: Lithium-sulfur battery, metallic sulfide, interconnected nanosheet, polysulfide adsorption, long cycle life, high sulfur loading.

Lithium-ion batteries (LIBs) have been extensively studied over the past decades and are now widely used in portable and other electronic devices.[1,2] New markets including the growing demand for green electric vehicles, however, require battery systems with even higher gravimetric/volumetric energy density as well as lower cost. Lithium-sulfur (Li-S) batteries, based on sulfur cathodes, are now considered one of the most promising candidates to replace LIBs, owing to their high theoretical specific capacity and energy density, low cost, natural abundance of sulfur and fewer safety concerns.[3-6] Nonetheless, the implementation of Li-S batteries still remains challenged because of low sulfur utilization and capacity fading, which originate from the insulating nature of sulfur/Li_2S, large volume expansion upon discharge and more importantly, the lithium polysulfide (LiPSs) shuttling between electrodes.[7-9]

Along with research to address electrolyte modification and anode protection, [10-12] much effort has been made to solve at least one of the three above-mentioned problems *via* improvement of the cathode. Initially nanostructured carbons with sophisticated pore structures were used to provide electron conductivity and physical entrapment of the LiPSs, including meso/micro-porous carbons,[13,14] porous carbon spheres,[15,16,17] carbon nanofiber interlayers,[18] or graphenes.[19,20] Introducing hosts that exhibit chemical interactions with LiPSs by using graphene oxides, [21,22] N-doped carbons[23,24] or N,S-doped carbons[25,26] has greatly improved electrochemical performance. However, achieving high doping concentration as well as uncompromised conductivity in modified carbons is challenging.[27] Non-conductive metal oxides or metal-organic frameworks with superior LiPSs adsorptivity have been used as additives or directly as the sulfur hosts,[28-31] but the power capability is compromised. Conductive Magnéli phases, indium tin oxide and MXene phases have been reported to promote the surface polysulfide redox reaction and spatially control the electro-deposition of Li_2S.[32 - 35] As well, layered semiconducting TiS_2[36] has been added to sulfur cathodes – and more recently – TiS_2 was used to coat Li_2S particles in order to alleviate polysulfide leakage into the electrolyte;[37] however, prolonged cycling of high-loading electrodes (>50 cycles) or long-term cycling of low-loading electrodes (>400 cycles) was not reported.

Herein, we describe a strong chemical interaction to confine LiPSs within a graphene-like Co_9S_8 nanosheet material that exhibits both metallic conductivity and hierarchical porosity. The thermal stability and electronic conductivity of cobalt sulfides are superior to most other metal sulfides.[38-40] Amongst these, Co_9S_8, a member of the Pentlandite family, a high-temperature peritectic phase in the Co-S phase diagram,[41] exhibits a particularly high room temperature conductivity of 0.29×10^3 S cm^{-1}.[42] It has been synthesized by low-temperature solvothermal techniques,[43,44] but these processes require long reaction time at elevated temperature, and yield conventional large crystallites. Here we demonstrate a rapid and scalable microwave solvothermal approach for the synthesis of a unique graphene-like Co_9S_8 with interconnected nanosheets that form 3D networks. Importantly we show that – in contrast to electrodes consisting of individualized Li_2S

particles coated with metal sulfides,[37] – the 3D network structure enables high sulfur loading electrodes with stable cycling. First-principles calculations and spectroscopic studies consistently demonstrate the coupled interaction of Co_9S_8 with Li_2S_n that relies on S_n^{2-}-$Co^{\delta+}$ and Li^+-$S^{\delta-}$ (of Co_9S_8) binding. We show that with these intrinsic active sites, the as-synthesized Co_9S_8 exhibits far superior LiPSs adsorptivity than "gold-standard" carbon materials, enabling electrodes with stable cycling behavior.

Microwave treatment utilizes a solvent dipole-microwave interaction leads to rapidly superheated regions triggering rapid nucleation and growth of particles.[45] This distinctive synthesis condition results in the formation of a long-range nanosheet structure of Co_9S_8 with a large pore volume. The X-ray diffraction (XRD) pattern (**Figure 1a**) can be indexed to cubic Co_9S_8 (F*m-3m*) with a lattice parameter of 9.930 Å (ICSD database #23929). A small amount of $Co_{1-x}S$ was also detected. The scanning electron microscopy (SEM) images in **Figure 1b, c** reveal an interconnected nanosheet structure, which gives rise to hierarchical porosity (see below). We believe that the sheets may result from binding of the triethylenetetramine solvent molecules onto specific Co_9S_8 crystallographic planes via Lewis acid-base (Co-N) chelation, leading to preferential growth along certain directions. This effect is even more pronounced by the rapid heating and nucleation under microwave conditions, which is known to direct specific particle morphologies[46] - so that here, a long-range nanosheet structure is formed. Such a 3D network is critical for maintaining the electrode integrity and thus allowing stable cycling for thick high-loading electrodes as discussed below.[47,48] The thin graphene-like structure is evident in the transmission electron microscopy image shown in **Figure 1d**. The high-resolution TEM (HRTEM) image of a single sheet shows lattice fringes with an interplaner spacing that exactly corresponds to the (111) plane of cubic Co_9S_8. N_2 adsorption/desorption analysis (**Figure 1e**) indicated a high Brunauer-Emmett-Teller (BET) surface area of 108 $m^2 g^{-1}$ and a very large pore volume of 1.07 $cm^3 g^{-1}$.

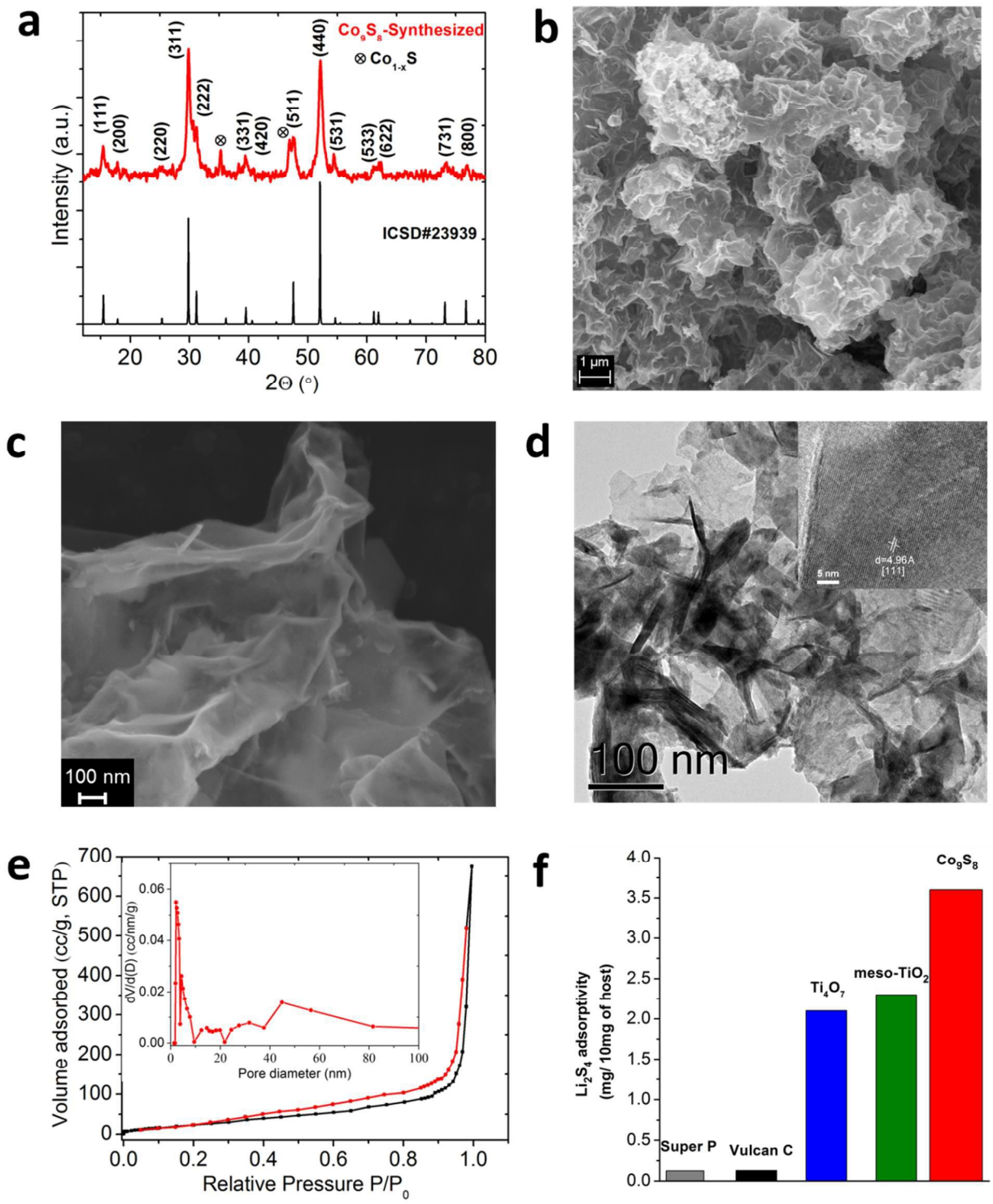

Figure 1. a-e) Physical characterization of the as-synthesized graphene-like Co_9S_8: a) XRD pattern (with indexed reflections), b,c) low- and high-magnification SEM images, d) TEM image (inset: HRTEM) and e) N_2 adsorption/desorption isotherm (inset: BJH pore size distribution). f) The Li_2S_4 adsorptivity of the Co_9S_8 measured by electrochemical titration, compared to meso-TiO_2, nanostructured Ti_4O_7, Vulcan™ carbon and Super P carbon.

A broad pore size distribution was observed, with the majority in the range of 1.2 - 10 nm and the remainder distributed over 10 - 80 nm, indicating a texture incorporating micro-, meso-, and macropores. This high surface area and pore volume

along with the hierarchical porosity are vital to exert high intrinsic LiPS adsorptivity and enhance electrolyte penetration across thick electrodes.

The LiPSs adsorptivity of Co_9S_8 was quantitatively evaluated by electrochemically titrating the residual polysulfide remaining in a LiPS solution solution after long contact with the Co_9S_8 host.[49] This is compared with traditional nonpolar carbons (Super P and Vulcan™ Carbon), a commercial mesoporous TiO_2 (meso-TiO_2), and nanostructured metallic Ti_4O_7,[33] in **Figure 1f**. Li_2S_4, synthesized from the reaction of sulfur and lithium superhydride, was employed as the representative polysulfide. Vulcan Carbon (VC, 260 m^2 g^{-1}) adsorbs only 0.15 mg of Li_2S_4 per 10 mg of material. The meso-TiO_2 (272 m^2 g^{-1}) and Ti_4O_7 (290 m^2 g^{-1}) adsorb twenty fold this amount, as reported previously.[49] However, the as-synthesized Co_9S_8 - despite possessing about one-third the surface area (108 m^2 g^{-1}) - adsorbs 50% more than either oxide. This demonstrates that Co_9S_8 has over five times the intrinsic LiPS adsorptivity (*i.e.* surface area normalized) of the titanium oxides.

To understand the nature of the bonding interaction of Co_9S_8 with LiPSs, first-principles calculations based on density functional theory were performed. We selected three representative surfaces that exhibit different surface Co/S ratios, (002), (202) and (008), in order to evaluate the contribution of surface Co atoms and S atoms in binding LiPSs. The (002) and (202) surfaces have a Co/S ratio of 1:4, 5:4 respectively and (008) is terminated entirely with Co atoms (see **Figure S1a, b, ESI** for details).[50] A four-layer slab model (with the bottom two layers fixed) was employed, where all three surface slabs contain the same number of total atoms. Non-polar graphitic carbon was used as a comparison, employing a two-layer graphite slab so that all substrates have very close supercell sizes. Short-chain Li_2S_2, along with longer-chain Li_2S_4 and the end-member sulfide Li_2S [51,52] were used to represent the LiPS molecules.

The fully relaxed geometries of Li_2S_2 binding for the surface slabs are shown in **Figure 2**. The absence of any specific bonding between Li_2S_2 and the graphite substrate leads to a low binding energy of 0.23 eV, which arises from the van der Waals interaction (**Figure 2a**).[52] In contrast, Li_2S_2 adsorbed on the Co_9S_8 surfaces exhibits slightly distorted geometries compared to the free Li_2S_2 molecule, indicating strong interaction (**Figure 2b-d**).

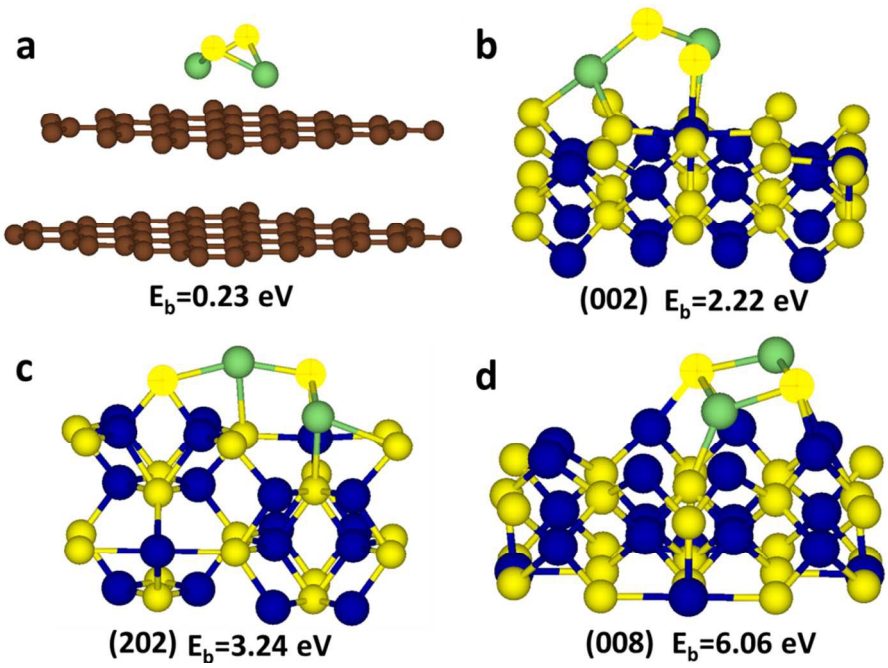

Figure 2. Schematic showing the most stable Li_2S_2 binding geometry configuration after full relaxation by first-principles calculations for the a) double-layer graphitic carbon, and four-layer Co_9S_8 b) (002), c) (202) and d) (008) surface slabs with the corresponding binding energy values labeled. Other less stable geometries at local minima are shown in **Figure S1, ESI**. Brown, blue, green and yellow 3D spheres represent C, N, Li and S (of Co_9S_8) atoms, respectively and 2D yellow circles represent S of Li_2S_2.

In all three cases, there is strong evidence for both S_2^{2-}-$Co^{\delta+}$ and Li^+-$S^{\delta-}$ (in Co_9S_8) binding, with energies above 2 eV. For example, on the (002) surface (**Figure 2b**), the Li atom prefers to bond with the three available neighboring sulfur (of Co_9S_8) atoms; and on the (008) surface (**Figure 2d**), the sulfur atoms (of Li_2S_2) prefer to bond with the Co atoms. In contrast to the previously reported observation of only Li-S (Li-O) binding between Li_2S_x and layered metal sulfide (oxide),[52] here we witness strong synergistic binding effect from both metal and sulfide ions. We believe this strong coupled interaction for binding LiPSs and the high-surface-area of the nanostructured Co_9S_8 contribute to its superior LiPSs binding capability. As reported by Zhang et al.,[52] van der Waals forces (VDW) are also important for evaluating the interaction of polysulfides (and sulfur) with substrates, especially for non-polar carbon surfaces. Inclusion of the VDW correction in the calculations yields binding energy values summarized in **Table 1**. With VDW forces included, the binding energy of Li_2S_2 with *all* substrates increased by 0.65~1.00 eV, demonstrating that it plays a role. The contribution of VDW forces to the total binding energy is greater for the non-polar graphite (70%) substrate than the Co_9S_8 substrate as expected (30%, 21%, 13% for the (002), (202) and (008) surfaces respectively). We also probed the longer chain polysulfide, Li_2S_4. Here, the binding of Li^+ to S of Co_9S_8, and that of terminal S to Co (if available) completely dominate the interaction, whereas the bridging "neutral" sulfur participates only on the Co-rich surface (008) **(Figure S2, ESI)**. We observed that the

binding energy values for Li_2S_4 on Co_9S_8 are a little lower than that of Li_2S_2 which only contains terminal sulfide atoms (**Table 1**) - consistent with what is reported in Ref. 52 - although both are much higher for Co_9S_8 than for graphite. The end member, Li_2S, exhibits a a 4 -7 fold higher binding energy on the Co_9S_8 surfaces (**Figure S2, ESI**).

Table 1. Summary of binding energies for different poly/sulfides on the surface of graphite and on three Co_9S_8 surfaces

E_b (eV)	Graphite	Co_9S_8 (002)	Co_9S_8 (202)	Co_9S_8 (008)
Li_2S	0.60	2.74	3.41	3.96
Li_2S_2	0.28	2.26	3.29	6.06
Li_2S_4	0.65	1.71	1.56	4.10
Li_2S_2-VdW	0.94	3.24	4.17	6.93

The crystallographic binding surface plays a very important role, as mentioned above. The binding energy of 2.22 eV for Li_2S_2 on the (002) surface (Co/S= 1:4) increases to 3.24 eV for the (202) surface (Co/S= 5:4) and further to 6.06 eV for the purely Co-terminated (008) plane which presents cobalt atoms in only tetrahedral coordination, which are undercoordinated at the surface. This binding energy (6.93 eV with van der Waals interactions included) is the highest reported for a lithium sulfide on a host surface to our knowledge, for example, exceeding that of Li_2S_2 on Ti_4O_7 (4.1 eV), or on TiS_2 (3.5 eV).[32,52] The correlation suggests that the Co-S interaction may play a more significant role in binding LiPSs than the Li-S interaction, since the three substrates have a similar supercell size and number of atoms. This finding enables a better understanding on the interaction mechanism for metal sulfide/oxides and provides guidance on fabricating host materials with preferred crystal faces.

X-ray photoelectron spectroscopy (XPS) has proven to be effective in probing the changes of chemical environments at the interface.[32,35] To further probe the underlying principles for the superior LiPSs adsorptivity for Co_9S_8, XPS studies were performed on the Co_9S_8-Li_2S_4 solid powder retrieved from the titration experiment described above. In the Li 1s spectrum of pristine Li_2S_4, a single component is observed at 55.4 eV (**Figure 3a**). Upon contact with Co_9S_8, this component shifts 0.5 eV towards lower binding energy (54.9 eV), suggesting a strong chemical interaction that results in electron transfer from the Co_9S_8 surface to the Li ions (**Figure 3b**). In the Co $2p_{3/2}$ spectrum, pristine Co_9S_8 exhibits two components (778.3

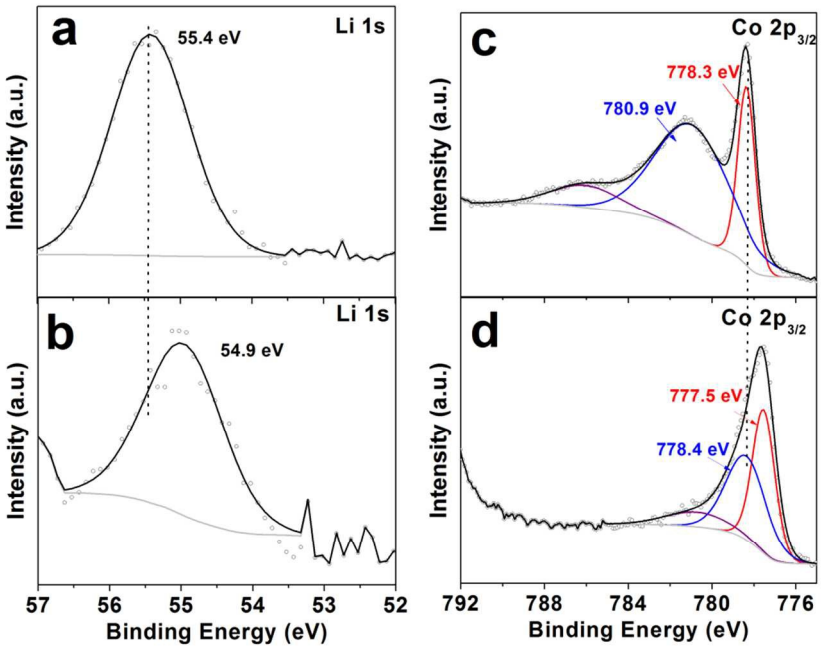

Figure 3. High-resolution XPS spectra of a, b) Li 1s and c, d) Co $2p_{3/2}$ regions for a) pristine Li_2S_4, c) pristine Co_9S_8, and b, d) Co_9S_8-Li_2S_4. Black circles and solid lines represent the experimental and overall fitted spectra, respectively.

eV and 780.9 eV) corresponding to two types of cobalt that occupy distinct lattice sites (octahedral and tetrahedral, respectively), with another broad Co 2p satellite peak (**Figure 3c**).[53,54] Upon contact with Li_2S_4, the Co $2p_{3/2}$ spectrum also shifts overall towards lower binding energy (**Figure 3d**), indicating electron transfer from Li_2S_4 molecules to the Co atoms. The tetrahedrally coordinated Co site shifts by 2.5 eV, about a factor of three more compared to the octahedral Co site, as expected, owing to its greater interaction based on the calculations shown above for the (008) surface (**Figure 2d**). This observation may extend to other transition metals.[55] We conclude that coupled electron transfer occurs (namely $S_2^{2-} \rightarrow Co^{\delta+}$ and $Li^+ \rightarrow S^{\delta-}$ (in Co_9S_8)), since the opposite configuration (*i.e.* $S_2^{2-} \rightarrow S^{\delta-}$, $Li^+ \rightarrow Co^{\delta+}$) would be hindered by electrostatics. In addition, the interaction of Li_2S_4 and Co_9S_8 led to the broadening of the S 2p XPS spectrum of Co_9S_8-Li_2S_4, suggesting contributions from different chemical states (**Figure S3, ESI)**, although no obvious peak shifts were observed for the S 2p components compared with the pure Co_9S_8 or Li_2S_4. Due to the presence of multiple and overlapping sulfur components,

further de-convolution of the S 2p spectra was not attempted. Overall, we demonstrate the synergistic interactions that exist on the Co_9S_8-Li_2S_4 interface by XPS studies, that are completely consistent with the first-principles calculations.

Sulfur cathodes based on Co_9S_8 were fabricated to investigate the practical benefits of its high LiPS adsorptivity, high conductivity and the interconnected nanosheet structure on the cycling stability of Li-S cells. Sulfur composites with a sulfur content of 75 wt% (Co_9S_8/S75) were prepared by melt-diffusion and the weight fraction was confirmed by thermogravimetric analysis (**Figure S4a, ESI**). The SEM image in **Figure S4b, ESI** shows that sulfur is evenly distributed over the Co_9S_8 sheets and no large sulfur particles are evident, promising good electrolyte infiltration and good electronic contact to the host. As a comparison, sulfur electrodes based on Vulcan™ carbon were also prepared (VC/S75, see **Figure S4c, ESI**). Li-S Cells with a typical sulfur loading of 1.5 mg cm^{-2} and an electrolyte/sulfur (E/S) ratio of 15: 1 (uL/mg) were first examined to enable comparison with previously published work;[22,23,32,34] high-loading electrodes with up to 4.5 mg cm^{-2} are described in the next section. All Li-S cells were initially cycled at a C/20 (1C = 1675 mAh g_S^{-1}) rate for conditioning before cycling at higher rates. Sulfur-free cells were built with pure Co_9S_8 cathodes and lithium metal anodes to exclude the electrochemical contribution from Co_9S_8. As shown in **Figure S5, ESI**, Co_9S_8 exhibits only capacitive behavior as indicated by its sloping profile, corresponding to a capacity of only 15-35 mA h g^{-1} in the typical Li-S voltage window.

The voltage profiles of the Co_9S_8/S75 electrodes at various C rates are shown in **Figure 4a**. High discharge capacities of 1130, 890, 895, and 863 mA h g^{-1} were achieved at C/20, C/2, 1C and 2C rates, respectively. It is noteworthy that virtually no capacity decrease was observed upon a rate increase from C/2 to 2C, indicating highly favorable power capability owing to the metallic properties of Co_9S_8. Prolonged cycling of the electrodes at all rates showed almost identical capacity retention over 400 cycles (**Figure 4b**). For example, at a 2C rate, a high capacity of 643 mA h g^{-1} was still obtained over 400 cycles, corresponding to 75% of the initial capacity. As shown in **Figure 4c,** the long-term cycling at a medium rate of C/2 demonstrates the superior

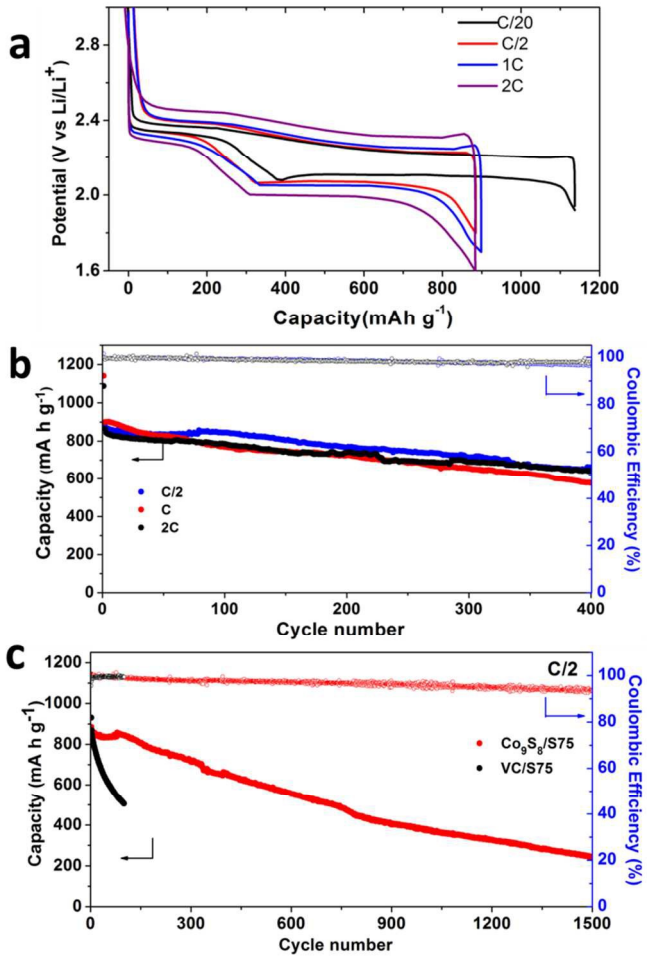

Figure 4. The cell voltage profiles of Co_9S_8/S75 electrodes at various C rates; b) prolonged cycling showing the discharge capacity retention of Co_9S_8/S75 electrodes at C/2, 1C and 2C rates over 400 cycles; d) the long-term cycling performance of Co_9S_8/S75 and VC/S75 electrodes at a C/2 rate under identical conditions. The Coulombic efficiency is shown on the right y-axis.

capacity retention of Co_9S_8 over the carbon-based VC/S75 electrode - the Co_9S_8/S75 electrode experienced an ultralow capacity fading rate of 0.045% per cycle, whereas the capacity of the VC/S75 electrodes faded rapidly over the first 100 cycles at a rate of 0.48% per cycle. We also investigated the evolution of the impedance of the Co_9S_8/S-75 cell over cycling, as shown in **Figure S6, ESI**. Upon the 1st cycle, the charge transfer resistance (high-frequency semi-circle) within the electrode decreased greatly (**Figure S6a, ESI**). However, over 40 cycles, the impedance showed negligible change (**Figure S6b, ESI**), indicating a good host/(poly)sulfide interface supported by the excellent conductivity of the Co_9S_8 substrate. The higher density of the Co_9S_8 host is also beneficial. The Co_9S_8/S75 composite has a higher compact density (2.9 g cm^{-3}) than that of a typical carbon or graphene-oxide composite at the same sulfur mass loading (1.8 g cm^{-3}). Accordingly, the Co_9S_8/S75 electrode exhibits a higher volumetric energy density of 1775 Wh/L at a C/5 rate, compared to a theoretical value of 1275 Wh/L for a carbon electrode, assuming all else is equal (see **ESI** for calculation details). Constructing high

sulfur loading electrodes is critical for building a high energy density Li-S battery for practical applications such as electric vehicles.[56] Electrodes were prepared with varied high sulfur loadings (2.5-4.5 mg cm^{-2}) to investigate the advantages of the 3D interconnected nanosheet structure of the nanostructured Co_9S_8. Styrene butadiene rubber / carboxymethyl cellulose binder and graphene carbon additives (4 wt%) were used to construct the electrodes. A lower E/S ratio of 10:1 (μL/mg) was used to minimize cell volume. The large-scale SEM image of the as-prepared electrodes shows a continuous surface **(Figure S3d, ESI)**. **Figure 5a** shows the voltage profiles of the electrodes at a C/20 rate. Areal capacities of 2.7, 3.5 and 4.3 mA h cm^{-2} were achieved for the electrodes with 2.5, 3.5 and 4.5 mg cm^{-2} loadings, respectively. There is no obvious increase of polarization (voltage difference between charge and discharge) upon increase of the sulfur loading, and the areal capacities

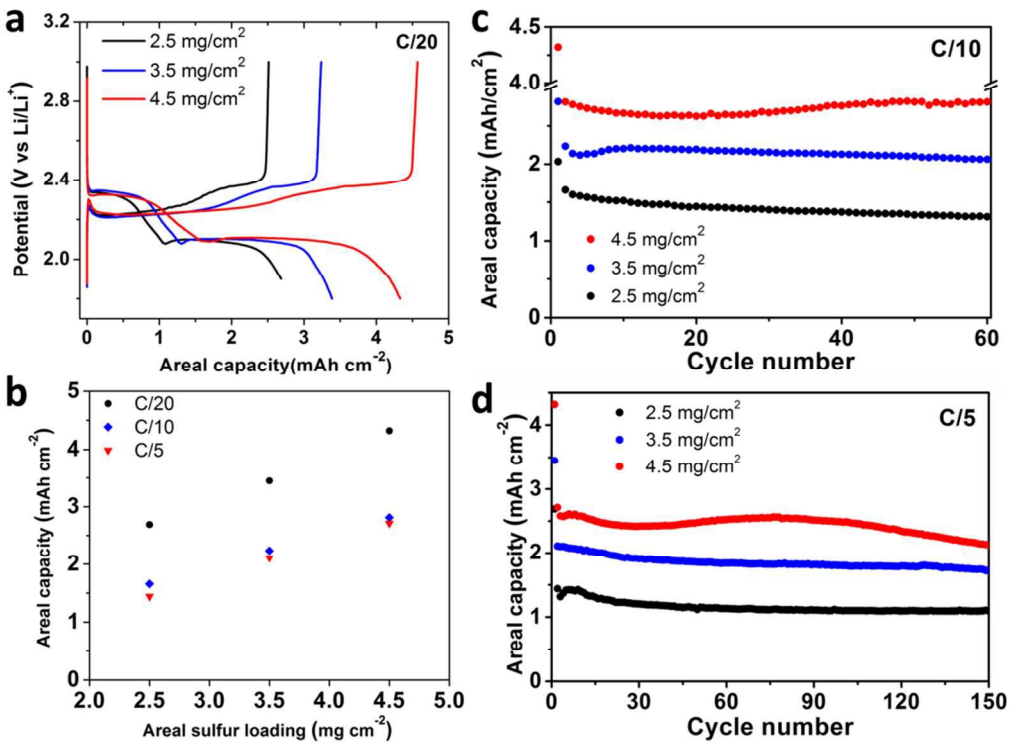

Figure 5. Electrochemical performance of the Co_9S_8/S75 high-loading electrodes, with all cells conditioned at C/20 for the first cycle. a) Initial-cycle voltage profiles of the electrodes with various loadings (2.5–4.5 mg cm^{-2}) at C/20 rate; b) comparisons of the areal discharge capacity of electrodes at C/5, C/10 and C/20 rates; c) the areal discharge capacity retention of high loading electrodes at C/10 for 60 cycles; d) the prolonged cycling performance of the Co_9S_8/S75 electrodes at C/5 for 150 cycles.

obtained at C/10 and C/5 are very close (**Figure 5b**), indicating excellent kinetics in spite of the high sulfur loading and thick electrodes. Deep cycling of the thick electrodes at a C/10 rate shows slight capacity increase followed by very stable retention for 60 cycles (**Figure 5c**). Prolonged cycling at a higher rate C/5 shows a similar trend with very stable cycling

over 150 cycles (**Figure 5d**). We note that although the areal capacity of 4.3 mA h cm^{-2} reported here (**Figure 5b, c)** is not the highest compared with some recently reported carbon-based electrodes with sophisticated cathode architectures,[23,47,48,57-59] our slurry-derived electrodes still exhibit very promising high areal capacity, with prolonged cycling stability achieved at high sulfur loading. However, existing problems regarding stability of the lithium metal anode at high current densities and deep stripping/plating remains to be solved before even longer-term cycling performance can be realized.[60]In conclusion, we have shown a scalable approach to synthesize a unique high-surface-area graphene-like Co_9S_8 material with hierarchical porosity. We reveal the underlying principles for the superior LiPS adsorptivity of Co_9S_8 over carbon materials via a combination of first-principles calculations and XPS studies. A synergistic dual-interaction based on $S_n^{2-} \rightarrow Co^{\delta+}$ and $Li^{+} \rightarrow S^{\delta-}$ exists between the metal sulfide-based host material and polysulfides. Using the Co_9S_8 based sulfur composite, an ultralow capacity fading rate of 0.045% per cycle over 1500 cycles was achieved. More importantly, high sulfur content electrodes, up to 4.5 mg cm^{-2} loading, were shown with stable cycling over 150 cycles, demonstrating their advantage in building high energy density Li-S batteries. This concept extends to other metal sulfide/oxides, and studies to find the optimal sulfur host that has both high electronic conductivity and polysulfide adsorption are underway.

Acknowledgements

We thank NRCan for generous financial support through their EcoEII program. NSERC is acknowledged for a underlying funding from the Discovery Grant and Canada Research Chair programs.

References

1 J. B. Goodenough, K.-S. Park, *J. Am. Chem. Soc.* 2013, **135**, 1167.

2 N.-S. Choi, Z. Chen, S. A. Freunberger, X. Ji, Y.-K. Sun, K. Amine, G. Yushin, L. F. Nazar, J. Cho, P. G. Bruce, *Angew. Chem.* 2012, **51**, 9994.

3 P. G. Bruce, S. A. Freunberger, L. J. Hardwick, J. M. Tarascon, *Nature Mater.* 2012, **11**, 19.

4 L. F. Nazar, M. Cuisinier, Q. Pang, *MRS Bull.* 2014, **39**, 436.

5 A. Manthiram, Y. Fu, Y.-S. Su, *Acc. Chem. Res.* 2012, **46**, 1125.

6 S. Evers, L. F. Nazar, *Acc. Chem. Res.* 2012, **46**, 1135.

7 Y. V. Mikhaylik, J. R. Akridge, *J. Electrochem. Soc.* 2004, **151**, A1969.

8 Y. Diao, K. Xie, S. Xiong, X. Hong, *J. Electrochem. Soc.* 2012, **159**, A421.

9 R. Elazari, G. Salitra, Y. Talyosef, J. Grinblat, C. Scordilis-Kelley, A. Xiao, J. Affinito, D. Aurbach, *J. Electrochem. Soc.* 2010, **157**, A1131.

10 Z. Lin, Z. Liu, W. Fu, N. J. Dudney, C. Liang, *Adv. Funct. Mater.* 2013, **23**, 1064

11 M. Cuisinier, P.-E. Cabelguen, B. Adams, A. Garsuch, M. Balasubramanian, L.F. Nazar, *Energy Environ. Sci.* 2014, **7**, 2697.

12 F. Wu, J. T. Lee, N. Nitta, H. Kim, O. Borodin, G. Yushin, *Adv. Mater.* 2015, **27**, 101.

13 X. Ji, K. T. Lee, L. F. Nazar, *Nature Mater.* 2009, **8**, 500.

14 R. Elazari, G. Salitra, A. Garsuch, A. Panchenko, D. Aurbach, *Adv. Mater.* 2011, **23**, 5641.

15 N. Jayaprakash, J. Shen, S. S. Moganty, A. Corona, L. A. Archer, *Angew. Chem.* 2011, **50**, 5904.

16 G. He, S. Evers, X. Liang, M. Cuisinier, A. Garsuch, L. F. Nazar, *ACS Nano* 2013, **7**, 10920.

17. K. Zhang, Q. Zhao, Z.L. Tao, J. Chen, *Nano Research*, 2013, **6**, 38.

18 Y.-S. Su, A. Manthiram, *Nature Commun.* 2012, **3**, 1166.

19 H. Wang, Y. Yang, Y. Liang, J. T. Robinson, Y. Li, A. Jackson, Y. Cui, H. Dai, *Nano Lett.* 2011, **11**, 2644.

20 S. Lu, Y. Cheng, X. Wu, J. Liu, *Nano Lett.* 2013, **13**, 2485.

21 L. Ji, M. Rao, H. Zheng, L. Zhang, Y. Li, W. Duan, J. Guo, E. J. Cairns, Y. Zhang, *J. Am. Chem. Soc.* 2011, **133**, 18522.

22 M. K. Song, Y. Zhang, E. J. Cairns, *Nano Lett.* 2013, **13**, 5891.

23 J. Song, T. Xu, M. L. Gordin, P. Zhu, D. Lv, Y.-B. Jiang, Y. Chen, Y. Duan, D. Wang, *Adv. Funct. Mater.* 2013, **24**, 1243.

24 W. Zhou, C. Wang, Q. Zhang, H. D. Abruña, Y. He, J. Wang, S. X. Mao, X. Xiao, *Adv. Energy Mater.* 2015, doi: 10.1002/aenm.201401752.

25 G. Zhou, E. Paek, G. S. Hwang, A. Manthiram, *Nature Commun.* 2015, **6**, 7760.

26 Q. Pang, J. Tang, H. Huang, X. Liang, C. Hart, K. C. Tam, L. F. Nazar, *Adv. Mater.* 2015, **27**, 6012.

27 S. Zhang, S. Tsuzuki, K. Ueno, K. Dokko, M. Watanabe, *Angew. Chem.* 2015, **54**, 1302.

28 X. Ji, S. Evers, R. Black, L. F. Nazar, *Nature Commun.* 2011, **2**, 325.

29 H. Kim, J. T. Lee, D.-C. Lee, A. Magasinski, W. Cho, G. Yushin, *Adv. Energy Mater.* 2013, **3**, 1308.

30 J. Zheng, J. Tian, D. Wu, M. Gu, W. Xu, C. Wang, F. Gao, M. H. Engelhard, J. G. Zhang, J. Liu, J. Xiao, *Nano Lett.* 2014, **14**, 2345.

31 X. Liang, C. Hart, Q. Pang, A. Garsuch, T. Weiss, L. F. Nazar, *Nature Commun*. 2015, **6**, 5682.

32 X. Tao, J. Wang, Z. Ying, Q. Cai, G. Zheng, Y. Gan, H. Huang, Y. Xia, C. Liang, W. Zhang, Y. Cui *Nano Lett.* 2015, **14***,* 5288.

33 Q. Pang, D. Kundu, M. Cuisinier, L. F. Nazar, *Nature Commun.* 2014, **5**, 4759.

34 H. Yao, G. Zheng, P. C. Hsu, D. Kong, J. J. Cha, W. Li, Z. W. Seh, M. T. McDowell, K. Yan, Z. Liang, V. K. Narasimhan, Y. Cui, *Nature Commun.* 2014, **5**, 3943.

35 X. Liang, A. Garsuch, L. F. Nazar, *Angew. Chem.* 2015, **54**, 3907.

36 A. Garsuch, S. Herzog, L. Montag, A. Krebs, K. Leitner, *ECS Electrochem. Lett.* 2012, **1**, A24.

37 Z. W. Seh, J. H. Yu, W. Li, P. C. Hsu, H. Wang, Y. Sun, H. Yao, Q. Zhang, Y. Cui, *Nature Commun.* 2014, **5**, 5017.

38 R. C. Hoodless, R. B. Moyes, P. B. Wells, *Catal. Today,* 2006, **114**, 377.

39 D. M. Pasquariello, R. Kershaw, J. D. Passaretti, K. Dwight, A. Wold, *Inorg. Chem.* 1984, **23**, 872.

40 Q. Wang; L. Jiao, Y. Han, H. Du, W. Peng, Q. Huan, D. Song, Y. Si, Y. Wang, H. Yuan, *J. Phys. Chem. C,* 2011, **115**, 8300.

41 Y. O. Chen, Y. A. Chang, *Metall. Trans. B*, 1978, **9**, 61.

42 N. Kumar, N. Raman, A. Z. Sundaresan, *Anorg. Allg. Chem*., 2014, **640**, 1069.

43 Z. Wang, L. Pan, H. Hu, S. Zhao, *CrystEngComm.,* 2010, **12**, 1899.

44 R. Jin, R. Liu, Y. Xu, G. Li, G. Chen, *J. Mater. Chem. A,* 2013, **1**, 7995.

45 I. Bilecka, M. Niederberger, *Nanoscale*, 2010, **2**, 1358.

46 G.B. Zeng, R. Caputo, D. Carriazo, L. Luo, M. Niederberger, *Chem. Mater*., 2013, **25**, 3399.

47 D. Lv, J. Zheng, Q. Li, X. Xie, S. Ferrara, Z. Nie, L. B. Mehdi, N. D. Browning, J.-G. Zhang, G. L. Graff, J. Liu, J. Xiao, *Adv. Energy Mater.* 2015, doi: 10.1002/aenm.201402290.

48 J. Song, M. L. Gordin, T. Xu, S. Chen, Z. Yu, H. Sohn, J. Lu, Y. Ren, Y. Duan, D. Wang, *Angew. Chem.* 2015, **54**, 4325.

49 C. J. Hart, M. Cuisinier, X. Liang, D. Kundu, A. Garsuch, L. F. Nazar, *Chem. Commun.* 2015, **51**, 2308.

50 R. A. Sidik, A. B. Anderson, *J Phy. Chem. B*, 2006, **110**, 936.

51 L. Wang, T. Zhang, S. Yang, F. Cheng, J. Liang, J. Chen, *J. Energy. Chem*. 2013, **22**,72.

52 Q. Zhang, Y. Wang, Z. W. Seh, Z. Fu, R. Zhang, Y. Cui, *Nano Lett.* 2015, **15**, 3780.

53 Z. Wang, L. Pan, H. Hu, S. Zhao, *CrystEngComm,* 2010, **12**, 1899.

54 Z. Li, W. Li, H. Xue, W. Kang, X. Yang, M. Sun, Y. Tang, C.-S. Lee, *RSC Adv.* 2014, **4**, 37180.

55 Q. Zhao, X. Hu, K. Zhang, N. Zhang, Y. Hu, J. Chen, *Nano Lett,* 2015, **15**, 721.

56 A. Rosenman, E. Markevich, G. Salitra, D. Aurbach, A. Garsuch, F. F. Chesneau, *Adv. Energy Mater.* 2015, doi: 10.1002/aenm.201500212

57 Z. Li, J. Zhang and X. W. D. Lou, *Angew. Chem.* 2015, doi: 10.1002/anie.201506972.

58 Q. Sun, X. Fang, W. Weng, J. Deng, P. Chen, J. Ren, G. Guan, M. Wang, H. Peng, *Angew. Chem.* 2015, **127**, 10685.

59 G. Zhou, E. Paek, G. S. Hwang, A. Manthiram, *Nature Commun.* 2015, **6**, 7760.

60 R. Cao, W. Xu, D. Lv, J. Xiao, J.-G. Zhang, *Adv. Energy Mater.* 2015, doi: 10.1002/aenm.201402273.

Conceptual insights:

We demonstrate that a metallic cobalt sulfide host material with a graphene-like interconnecting nanosheet architecture enables long life, high sulfur content (75 wt%), and high areal loading lithium-sulfur batteries. Lithium-sulfur batteries are considered as the next-generation electrochemical system to replace conventional lithium-ion batteries due to their high theoretical capacity and low cost. However, capacity fading and inferior high-loading performance exist that result from the unique dissolution/re-precipitation chemistry of the sulfur species in the cell. Development of advanced sulfur host materials that embrace both high electronic conductivity and strong chemisorption towards the polysulfide intermediate species is crucial. By combining in-depth first-principles computation and spectroscopic analysis, we unravel the underlying nature of the coupled interactions between lithium polysulfides and metal sulfide/oxide, providing guidance for identification of efficient sulfur hosts. Importantly, we show that the long-range three-dimensionally interconnected architecture of the nanostructured metallic host allows high areal loading electrodes to be fabricated with stable cycling performance.

Figure for Table of Contents

TOC: